Fuel 242 (2019) 355–361

Contents lists available at ScienceDirect

Fuel

journal homepage: www.elsevier.com/locate/fuel

Full Length Article

Study on competitive absorption of SO_3 and SO_2 by calcium hydroxide

Kejia He, Qiang Song*, Zhennan Yan, Na Zheng, Qiang Yao

Key Laboratory of Thermal Science and Power Engineering of Ministry of Education, Department of Energy and Power Engineering, Tsinghua University, 10084 Beijing, China

ARTICLE INFO

Keywords:
SO_3
SO_2
$Ca(OH)_2$
Competitive absorption
Ionic diffusion

ABSTRACT

Alkaline injection is an effective way to control the emission of high concentration SO_3 caused by the use of high-sulfur coal and selective catalytic reduction (SCR), but its performance is affected by the competitive absorption of SO_2. A fixed-bed reactor was used to study the competitive absorption of SO_3 and SO_2 by $Ca(OH)_2$. The dynamic absorption curves in different atmospheres were obtained, the intermediate products were characterized, and the competitive absorption mechanism was discussed. The absorption of SO_3 and SO_2 consists of the chemical kinetics-controlled and product layer diffusion-controlled stages. In the chemical kinetics-controlled stage, the SO_3 and SO_2 removal efficiencies were around 90% and 55% at first and then decreased; the SO_3 selectivity was around 0.1 at first and then increased. In the product layer diffusion-controlled stage, the SO_3 removal efficiency gradually decreased but kept greater than 10%, while the SO_2 removal efficiency deceased to zero; the SO_3 selectivity continued to increase and reached 0.31 at most when SO_2 absorption ceased. There existed significant competition between SO_3 and SO_2 absorption. The increasing SO_3 concentration promoted the SO_3 absorption and the increasing SO_2 concentration decreased it. The absorption of SO_3 increased the intensity of the SO_4^{2-} band, decrease the intensity of the SO_3^{2-} band, and made the product layer more compact. The possibility of SO_3 reacting with the components ($CaSO_3$, $CaSO_4$ and $CaCO_3$) on the reacted $Ca(OH)_2$ surface was analyzed. Ionic diffusion was proposed as the main mechanism of the continuous SO_3 absorption after the formation of a dense product layer.

1. Introduction

The in-furnace combustion and catalytic oxidation of SCR lead to a 2% oxidation of SO_2 to SO_3 in coal-fired units [1–3]. The SO_3 concentration reaches 30 ppm or more when burning high-sulfur coal. This SO_3 concentration is enough to cause serious problems, such as increasing the acid dew point of the flue gas, corroding the air preheater (APH) and aggravating stack opacity and smog [1,4–8]. For example, the number concentration of sulfuric acid droplets may reach $10^8\,cm^{-3}$ after the wet flue gas desulfurization (WFGD) [9,10], and the blue plume appears at the stack when SO_3 concentration exceeds 5 ppm [11]. As a result, SO_3 controlling is of great significance for the stable operation of coal-fired units and the reduction of pollutants.

There are three main kinds of control methods for SO_3 emissions. The first is to adjust the combustion conditions. Fleig et al. found that the SO_3 concentration reduced by 30–40% with a reduction of combustion temperature or oxygen concentration by 60 °C or 5%, respectively [12], thus revealing a limited removal efficiency. The second is the SO_3 synergistic removal of the precipitator or the WFGD. Previous reports found that the baghouse filter, the electrostatic precipitator, the wet electrostatic precipitator and the WFGD had some synergistic removal effect on SO_3 [13–16], but the APH corrosion cannot be solved. The third control method is to spray alkaline absorbents into the flue gas to achieve solidification removal of the strongly acidic gaseous SO_3.

There are three feasible injection positions for the alkaline absorbents, which are in the furnace, between the SCR and the APH, and between the APH and the precipitator. Blythe et al. injected the $Mg(OH)_2$ slurry into the furnace and found that the SO_3 removal efficiency was 90% with a Mg/S molar ratio of 3.5:1 [17]. However, the in-furnace SO_3 removal is incapable of the SCR formed SO_3. Wahlco injected ammonia between the APH and the precipitator and observed a 95 + % SO_3 removal efficiency at an N/S molar ratio of 1:1–2:1 [18]. Injecting ammonia between the APH and the precipitator cannot alleviate the APH corrosion, and products (ammonium sulfate or ammonium bisulfate) will affect the fly ash disposal/reuse. In summary, it is more feasible to inject alkaline absorbents between the SCR and the APH, which can remove both the in-furnace and the SCR formed SO_3 and alleviate the APH corrosion.

Some laboratory research and engineering tests have been carried out to control SO_3 between the SCR and the APH. In the laboratory

* Corresponding author.
E-mail address: qsong@tsinghua.edu.cn (Q. Song).

https://doi.org/10.1016/j.fuel.2019.01.046
Received 5 November 2018; Received in revised form 11 December 2018; Accepted 7 January 2019
Available online 15 January 2019
0016-2361/ © 2019 Elsevier Ltd. All rights reserved.

research, previous researchers conducted a series of experiments on the reactivity of various metal oxides with just SO_3 in the reactant gas and found the order of the reactivity was Mg < Ca < Na < K [19,20]. Considering the cost and the reactivity, more researches focused on the calcium-based sorbents [21–25], which showed good deSO_3 performance. Wang et al. found the SO_3 removal efficiency was 99% with the $Ca(OH)_2$ of a 3 μm particle size [21]. In the engineering tests, Martin Marietta injected MgO in several full-scale tests and showed a 65% SO_3 removal efficiency at an Mg/S molar ratio of 1.5:1 [26]. However, the effect of other acid gases (such as SO_2) on SO_3 absorption had not been studied.

The SO_3 and SO_2 selectivity by the absorbent directly influenced the removal efficiency of SO_3 and the conversion of absorbents by absorbing SO_3, but there are no studies on the competitive reaction between SO_3 and SO_2. In the dry desulfurization process, some scholars found that CO_2 had a great influence on the effective calcium utilization efficiency of the desulfurizer at 540–582 °C [27]. During the CO_2 capture process, the CO_2 absorption reduced in the presence of SO_2, especially using high-efficiency absorbents or increasing temperature [28–30]. Because the concentration and acidity of SO_3 and SO_2 are similar to those of SO_2 and CO_2, the competitive absorption between SO_3 and SO_2 may exist during the desulfurization process.

The alkaline absorbent injection between the SCR and the APH can effectively control SO_3, and the competitive absorption of SO_3 and SO_2 has an important influence on the removal efficiency and cost. A fixed-bed reactor was applied to study the competitive absorption experiments of $Ca(OH)_2$ on SO_3 and SO_2. The dynamic absorption curve was obtained, including the conversion of $Ca(OH)_2$ by absorbing SO_3 and SO_2, SO_3 removal efficiency and the selectivity. The physical and chemical properties of the intermediate products will be characterized. The competitive reaction mechanism will be proposed combined with verification experiments.

2. Experiment

2.1. Experimental setup

A SO_X absorption experiment system is shown in Fig. 1. The entire experimental system consisted of a gas distribution system, a SO_3 generation reactor, a SO_X absorption reactor and an analytical instrument.

The gas distribution system consisted of the gas cylinders, pressure reducing valves, mass flow controllers and connecting lines. The standard and high purity gases used in the experiments were supplied by the Air Liquide (China) Holding Co., Ltd. One mixed gas (SO_2, O_2, balance gas was N_2) generated a high concentration of SO_3 by the SO_3 reactor, and the other mixed gas (SO_2, N_2 as balance) was used to dilute the high concentration of SO_3 to obtain the desired low concentration of SO_3. The total flow rate was 500 Nml/min. The desired SO_3 and SO_2 concentrations were obtained by adjusting the amount of the catalyst, the O_2 concentration was 5%, and the balance gas was N_2.

The quartz reactors of the SO_3 generation reactor and the SO_X absorption reactor comprised an inner tube and an outer tube. The inner tube of the SO_3 generation reactor was 13 mm in diameter, and the V_2O_5/TiO_2 catalyst was placed at the bottom of the inner tube, fixing with the analytically pure quartz wool. The inner tube of the SO_X absorption reactor consisted of a removable quartz basket (internal diameter of 15 mm), which was connected to the underlying inner tube by a scrub connection. A quartz filter membrane (MK360, Sweden) was laid at the bottom of the quartz basket to support the 100 mg $Ca(OH)_2$. The quartz basket was located in the constant temperature zone at a reaction temperature of 300 °C with an error of less than 2 °C.

The gas analysis instrument was a Fourier transform infrared spectroscopy (FTIR, Nicolet 6700, USA) for the on-line measurement of SO_2 concentration. The relative standard deviation of SO_2 concentration measured by the FTIR was 0.5%. To prevent FTIR corrosion, the gas passed through a U-tube stuffed with analytically pure quartz wool before entering the FTIR to filter out possible sulfuric acid droplets.

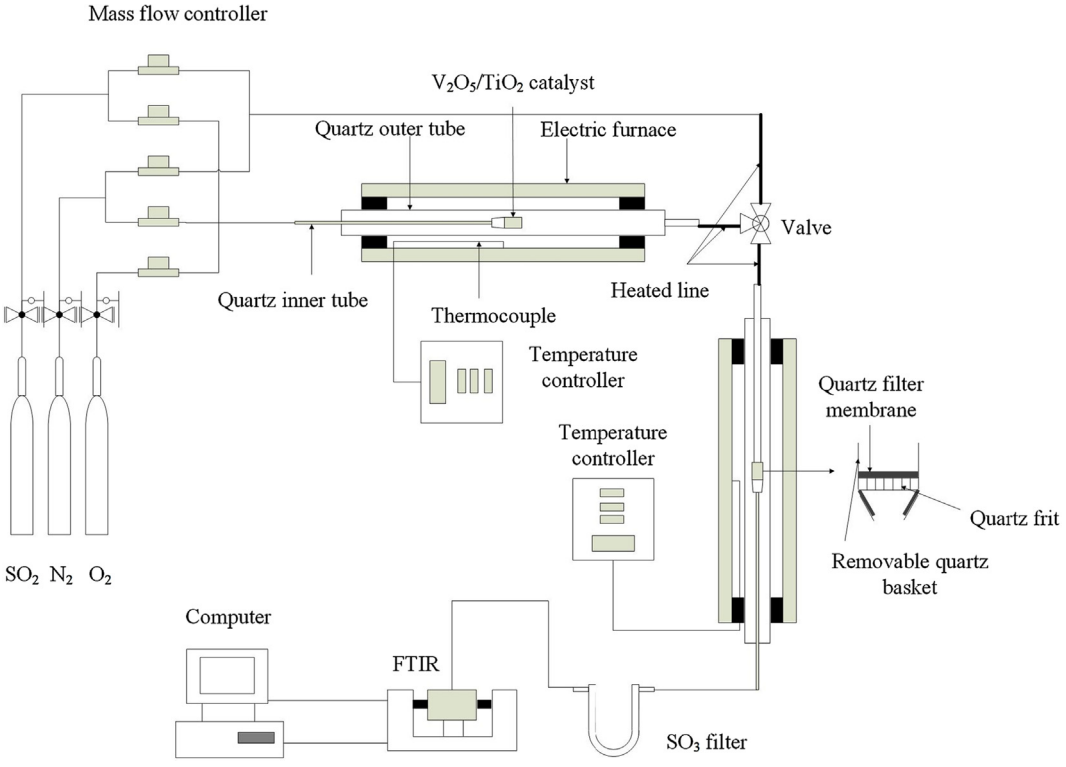

Fig. 1. Schematic of the SO_X absorption system.

Table 1
Properties of $Ca(OH)_2$.

$Ca(OH)_2$ content (%)	95
$CaCO_3$ content (%)	5
Average particle diameter (μm)	72
Specific surface area (m^2/g)	19.9
Specific pore volume (cm^3/g)	0.077
Average pore diameter (nm)	15.5

2.2. Materials

Analytically pure $Ca(OH)_2$ produced by Sinopharm Chemical Reagent Co., Ltd. was used in the experiment and the properties of the $Ca(OH)_2$ are listed in Table 1.

The V_2O_5/TiO_2 catalyst is used to catalyze the oxidation of SO_2 to SO_3. Ethanedioic acid dihydrate ($C_2H_2O_4{\cdot}2H_2O$), ammonium metavanadate (NH_4VO_3) and titanium dioxide (TiO_2) were added to the deionized water at a $C_2H_2O_4{\cdot}2H_2O/NH_4VO_3/TiO_2$ mass ratio of 5:2:10. The catalyst was mixed at 60–70 °C, dried in an oven at 100–105 °C and then calcined for 3 h at 250 °C and 450 °C, respectively, in an air atmosphere.

2.3. Method

SO_2 absorption can be obtained by integrating the inlet and outlet SO_2 concentration difference of the SO_x absorption reactor with the reaction time. SO_3 absorption can be acquired by the isopropanol absorption method and the controlled condensation method. However, the above two methods need a sufficient sampling amount, and the sampling time is more than 30 min, which is difficult to be used for the real-time measurement of dynamic SO_3 absorption processes. The PENTOL SO_3 analyzer shortened the sampling time, but the measurement accuracy was influenced by the incomplete absorption of the sample, the SO_2 oxidation, the side reaction of SO_3 and the isopropanol evaporation [31]. To determine the dynamic SO_3 absorption amount, a novel method that combined offline analysis of sulfur content in a solid sample by a thermogravimetric analyzer (TGA) and online measurement of SO_2 concentration was established. After a certain period of reaction, the absorbent sample contained desulfurization products ($CaSO_3$ and $CaSO_4$), unreacted $Ca(OH)_2$, and a small amount of impurities ($CaCO_3$) [32]. First, the sample was heated in an air atmosphere at 550 °C for 20 min to completely oxidize $CaSO_3$ to $CaSO_4$ and exclude the $CaSO_3$ disproportionation reaction. Then, the oxidized sample ($Ca(OH)_2$, $CaCO_3$ and $CaSO_4$) was placed in a TGA (Mettler Toledo TGA/DSC 3+, Switzerland) and heated to 1300 °C for 10 min at a heating rate of 30 °C/min. Since $CaSO_4$ undergoes a decomposition reaction as shown in Eq. (1) at 1200–1300 °C, the total sulfur content in the sample can be calculated according to the weight loss rate, subtracting the SO_2 absorption amount to obtain the SO_3 absorption amount.

$$CaSO_4 \xrightarrow{1200-1300^{\circ}C} CaO + SO_2 + \frac{1}{2}O_2 \quad (1)$$

The samples reacted in the SO_x absorption reactor for different times (1/2/5/10/20/30/60 min) were analyzed by the above method to obtain SO_3 and SO_2 absorption amounts with the reaction time. The relative standard deviation of SO_3 absorption amount measured by this method was related to the SO_3 absorption amount and decreased with the increase in the SO_3 absorption amount. For example, the relative standard deviation was around 5% when the conversion of $Ca(OH)_2$ by absorbing SO_3 was around 0.74% and decreased to 2% when the conversion of $Ca(OH)_2$ by absorbing SO_3 was around 2.22%.

The conversion of $Ca(OH)_2$ by absorbing SO_2, R_{SO_2}, the conversion of $Ca(OH)_2$ by absorbing SO_3, R_{SO_3}, and the conversion of $Ca(OH)_2$ by absorbing SO_X, R_{SO_X}, are defined in Eqs. (2), (3) and (4), respectively.

$$R_{SO_2} = \frac{N_{SO_2}}{N_{Ca(OH)_2}} \quad (2)$$

$$R_{SO_3} = \frac{N_{SO_3}}{N_{Ca(OH)_2}} \quad (3)$$

$$R_{SO_X} = \frac{N_{SO_2} + N_{SO_3}}{N_{Ca(OH)_2}} \quad (4)$$

where N_{SO_2} and N_{SO_3} are respectively the SO_2 and SO_3 absorption amounts in units of mol; $N_{Ca(OH)_2}$ is the original $Ca(OH)_2$ amount in units of mol.

The SO_2 removal efficiency, α_{SO_2}, is defined in Eq. (5).

$$\alpha_{SO_2} = \frac{C_{SO_2,in} - C_{SO_2,out}}{C_{SO_2,in}} \quad (5)$$

where $C_{SO_2,in}$ and $C_{SO_2,out}$ are respectively the SO_2 concentrations at the inlet and outlet of the reactor in units of ppm.

Since the real-time SO_3 concentrations at the inlet and outlet of the reactor cannot be measured directly, the SO_3 removal efficiency, α_{SO_3}, is determined as in Eq. (6).

$$\alpha_{SO_3,\frac{(t_2+t_1)}{2}} = \frac{N_{SO_3,t_2} - N_{SO_3,t_1}}{\frac{C_{SO_3,in} \times Q \times (t_2 - t_1)}{22.4}} \quad (6)$$

where t_1 and t_2 are two adjacent sampling moments in units of minute; N_{SO_3,t_1} and N_{SO_3,t_2} are respectively the SO_3 absorption amounts in units of mol at t_1 and t_2; $C_{SO_3,in}$ is the SO_3 concentration at the inlet in unit of ppm; Q is the inlet gas flow rate in unit of L/min.

The SO_3 selectivity, S_{SO_3}, is defined in Eq. (7).

$$S_{SO_3} = \frac{N_{SO_3}}{N_{SO_3} + N_{SO_2}} \quad (7)$$

The Fourier transform infrared spectroscopy (FTIR, Nicolet 6700, USA), Scanning Electron Microscope (SEM, ZEISS Merlin, Germany) and Surface Area and Porosity Analyzer (Micrometrics ASAP 2020, USA) were used to observe the sulfur-containing functional groups, the surface morphology, the specific surface area and pore structures of the original $Ca(OH)_2$ and the desulfurization products under different experimental conditions, respectively.

3. Results and discussion

3.1. Co-absorption of SO_2 and SO_3 by $Ca(OH)_2$

The pure SO_3 cannot be produced by the catalytic oxidation method. To compare the effects of SO_2 and SO_3 absorption on each other, experiments were carried out in five atmospheres (2000 ppm SO_2, 1000 ppm SO_2 + 100 ppm SO_3, 2000 ppm SO_2 + 100 ppm SO_3, 3000 ppm SO_2 + 100 ppm SO_3, 2000 ppm SO_2 + 200 ppm SO_3). Fig. 2 shows the conversion of $Ca(OH)_2$ by absorbing SO_X (a) and the conversion of $Ca(OH)_2$ by absorbing SO_3 or SO_2 (b) as a function of time at each atmosphere.

In Fig. 2(a), the conversion of $Ca(OH)_2$ by absorbing SO_x increased rapidly in the initial stage and then turned to slowly increase in the later stage, which corresponded to chemical kinetics control and product layer diffusion control, respectively [33]. In the chemical kinetics-controlled stage, the conversion of $Ca(OH)_2$ by absorbing SO_x increased with the increasing SO_3/SO_2 concentration. When the process transited from chemical kinetics-controlled to product layer diffusion-controlled, the increasing SO_2 concentration had little influence on the increase of the conversion, while the increasing SO_3 concentration increased the conversion obviously.

In Fig. 2(b), the conversion of $Ca(OH)_2$ by absorbing SO_3 or SO_2 showed a rapid increase in the chemical kinetics-controlled stage. In the product layer diffusion-controlled stage, the conversion of $Ca(OH)_2$ by absorbing SO_3 kept increasing with a slower rate, while the conversion

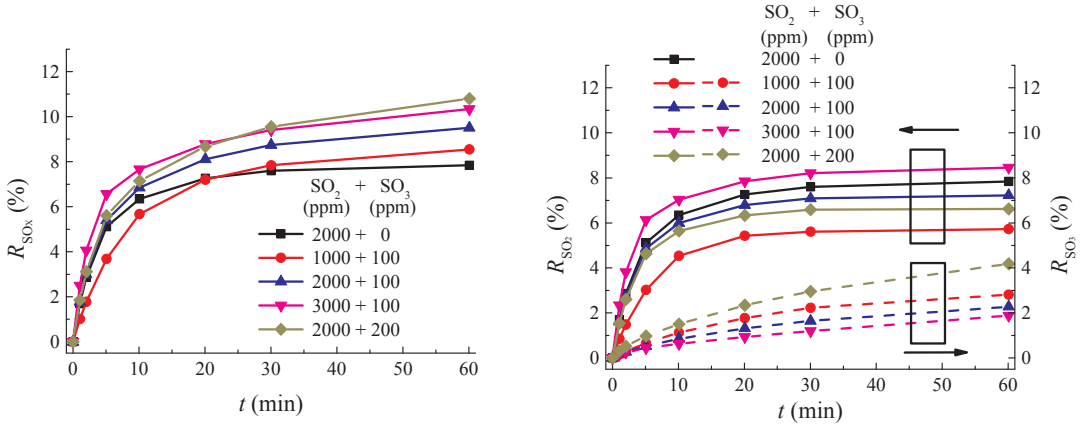

(a) The conversion of $Ca(OH)_2$ by absorbing SO_X (b) The conversion of $Ca(OH)_2$ by absorbing SO_3 or SO_2

Fig. 2. The conversion of $Ca(OH)_2$ by absorbing SO_x (a) and the conversion of $Ca(OH)_2$ by absorbing SO_3 or SO_2 (b) as a function of time.

of $Ca(OH)_2$ by absorbing SO_2 gradually reached a constant after approximately 30 min. In the chemical kinetics-controlled stage, the increasing SO_2 concentration slightly decreased the conversion of $Ca(OH)_2$ by absorbing SO_3 because of the sufficient active sites at the beginning, and significantly decreased the conversion of $Ca(OH)_2$ by absorbing SO_3 in the later stage due to the competitive consumption of the active sites. In the product layer diffusion-controlled stage, the increasing SO_2 concentration continued to decrease the conversion of $Ca(OH)_2$ by absorbing SO_3 at the beginning, and its effect weakened till the cessation of the SO_2 absorption. The increasing SO_3 concentration increased the conversion of $Ca(OH)_2$ by absorbing SO_3, and decreased the conversion of $Ca(OH)_2$ by absorbing SO_2 with a slight decrease in the chemical kinetics-controlled stage and a significant decrease in the product layer diffusion-controlled stage.

The above experimental results showed an obvious competition between SO_3 and SO_2 absorption. The absorption selectivity of $Ca(OH)_2$ for SO_3 as a function of time are shown in Fig. 3. In the initial chemical kinetics-controlled stage, the active sites consumed by SO_2 and SO_3 were negligible compared to the original sufficient active sites on the $Ca(OH)_2$ surface, thus the absorption rates of SO_2 and SO_3 were almost constant, causing an invariant SO_3 selectivity. The SO_3 selectivity of the four atmospheres (1000 ppm SO_2 + 100 ppm SO_3, 2000 ppm SO_2 + 100 ppm SO_3, 3000 ppm SO_2 + 100 ppm SO_3 and 2000 ppm SO_2 + 200 ppm SO_3) were 0.16, 0.09, 0.06 and 0.17, respectively, and the values were small due to the large difference in the reactant gas concentration. In the later chemical kinetics-controlled stage, some active sites on the $Ca(OH)_2$ surface were consumed due to the continuous absorption, and the competition in the reactions of SO_3 and SO_2 with the limited active sites became significant. The SO_3 selectivity increased due to the higher activity of SO_3. In the product layer diffusion-controlled stage, the $Ca(OH)_2$ surface was covered by the SO_x absorption products, the diffusion of the reactant gas through the product layer decelerated the SO_3 absorption, and the increase rate of the SO_3 selectivity began to slow down. The SO_3 selectivity reached 0.28, 0.19, 0.13 and 0.31 after 30 min (when the SO_2 absorption stopped), and 0.33, 0.24, 0.18 and 0.39 after 60 min, for the atmospheres of 1000 ppm SO_2 + 100 ppm SO_3, 2000 ppm SO_2 + 100 ppm SO_3, 3000 ppm SO_2 + 100 ppm SO_3 and 2000 ppm SO_2 + 200 ppm, respectively. The increasing SO_3 concentration and the decreasing SO_2 concentration increased the SO_3 selectivity.

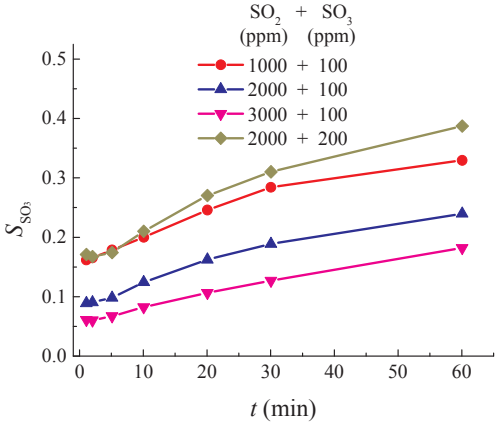

Fig. 3. The absorption selectivity of $Ca(OH)_2$ for SO_3 as a function of time.

Fig. 4 shows the SO_3 removal efficiency (a) and SO_2 removal efficiency (b) as a function of time. In the initial chemical kinetics-controlled stage, the SO_3 and SO_2 removal efficiencies were around 90% and 55%, respectively, but decreased rapidly and then slowly. After 30 min, the SO_3 removal efficiency was still greater than 10%, while the SO_2 removal efficiency tended to be zero. The increasing SO_2 concentration decreased the SO_3 removal efficiency. In the chemical kinetics-controlled stage, the increasing SO_2 concentration slightly decreased the SO_3 removal efficiency at the beginning, and significantly decreased the SO_3 removal efficiency in the later stage. In the product layer diffusion-controlled stage, the increasing SO_2 concentration continued to decrease the SO_3 removal efficiency at the beginning, and no longer affected the SO_3 removal efficiency in the later stage due to the cessation of the SO_2 absorption. The increasing SO_3 concentration decreased the SO_2 removal efficiency with a slight decrease in the chemical kinetics-controlled stage and an obvious decrease in the product layer diffusion-controlled stage.

3.2. Characterization of co-absorbed samples of SO_2 and SO_3 by $Ca(OH)_2$

Fig. 5 shows the functional groups of the desulfurization products at different reaction times (2/10/60 min) at 300 °C. The simulated flue gas of Fig. 5(a) was 2000 ppm SO_2. The band at 3641 cm^{-1} was due to the OH^- of the original $Ca(OH)_2$ and the bands at 1435 cm^{-1} and 876 cm^{-1} were due to the CO_3^{2-} of the impurities ($CaCO_3$). With the SO_2 absorption on the $Ca(OH)_2$ surface, bands of SO_4^{2-} and SO_3^{2-} appeared at 1142 cm^{-1} and 957 cm^{-1}, respectively [27,34], indicating that $Ca(OH)_2$ reacted with SO_2 to form $CaSO_3$, and a small amount of $CaSO_3$ was oxidized to $CaSO_4$ in the presence of 5% O_2. As the reaction time increased, the content of $CaSO_3$/$CaSO_4$ increased, and the corresponding bands became stronger. The simulated flue gas of Fig. 5(b) was 2000 ppm SO_2 + 100 ppm SO_3. After the addition of SO_3, the intensity of the SO_4^{2-} band increased while the intensity of the SO_3^{2-} band decreased compared with the SO_2 absorption.

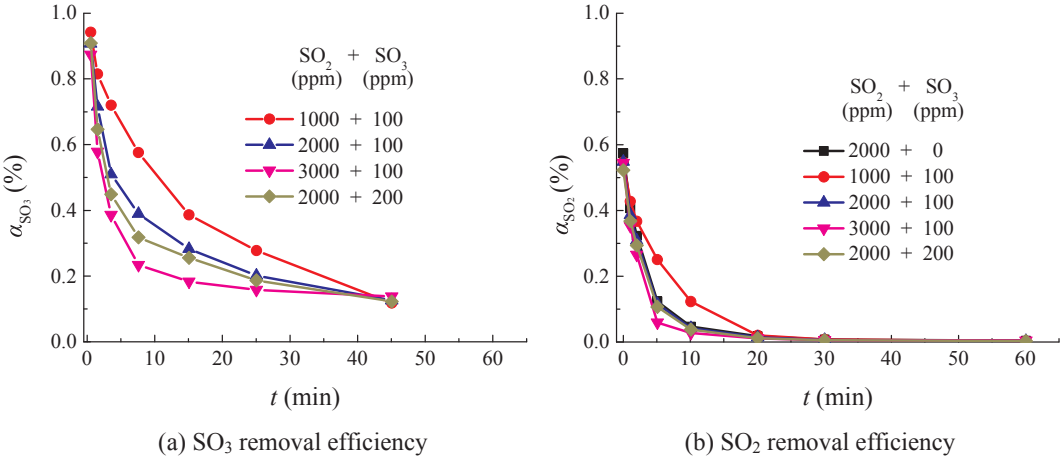

(a) SO_3 removal efficiency (b) SO_2 removal efficiency

Fig. 4. The SO_2 removal efficiency (a) and SO_3 removal efficiency (b) by $Ca(OH)_2$ as a function of time.

Fig. 6 presents the surface morphology of the original $Ca(OH)_2$ and the desulfurization products. As shown in Fig. 6(a), the original $Ca(OH)_2$ had a sheet-like structure with a smooth surface and a small number of protrusions, which might correspond to $CaCO_3$ impurities. Fig. 6(b) shows the surface morphology of $Ca(OH)_2$ absorbed 2000 ppm SO_2 for 60 min. With the formation of $CaSO_3$ and a small amount of $CaSO_4$, a large number of granular small protrusions cover the $Ca(OH)_2$ surface. Fig. 6(c) shows the surface morphology of $Ca(OH)_2$ absorbed 2000 ppm SO_2 + 100 ppm SO_3 for 60 min. After the addition of SO_3, a large amount of $CaSO_4$ was formed, and the small protrusions originally formed by the absorption of SO_2 disappeared and were replaced by the large and relatively smooth protrusion. The structure of the desulfurization products was denser.

The specific surface area and pore structures of the original $Ca(OH)_2$ and the desulfurization products were analyzed by Surface Area and Porosity Analyzer, as shown in Table 2. Because of the formation of the desulfurization products, the specific surface area and specific pore volume of the sample decreased, and the decreases were more significant in the presence of SO_3. This was consistent with the observations of the SEM.

3.3. Competitive absorption mechanism of $Ca(OH)_2$ on SO_2 and SO_3

The dynamic SO_2 absorption process transited from the chemical kinetics-controlled stage to the product layer diffusion-controlled stage, and finally stopped SO_2 diffusion due to the excessive diffusion resistance of the product layer. SO_3 absorption should also undergo a similar process, and since the SO_3 molecule is larger than SO_2, the SO_3 product layer diffusion resistance should be greater, and the SO_3 absorption in the product layer diffusion-controlled stage should end earlier. However, the actual situation was that the conversion of $Ca(OH)_2$ by absorbing SO_3 experienced two stages: a rapid increase and a slight increase. The SO_2 absorption had almost stopped, while the SO_3 absorption still continued. There may be two types of reasons for this phenomenon: one was that some components on the reacted $Ca(OH)_2$ surface continued to react with SO_3, and the other was that the product layer diffusion mechanism had transformed from the SO_3 product layer diffusion to the ionic diffusion. The components on the reacted $Ca(OH)_2$ surface contained $CaSO_3$, $CaSO_4$, and a small amount of impurities ($CaCO_3$). The possibility of SO_3 reacting with these components was analyzed one by one.

First, the possibility of SO_3 reacting with $CaSO_3$ to replace SO_2 was verified. A total of 100 mg $Ca(OH)_2$ was placed in the SO_X absorption reactor at 300 °C, and the reaction gas of 2100 ppm SO_2 (5% O_2, N_2 as balance) was supplied for 60 min. When the SO_2 concentrations at the outlet of the reactor was equal to the inlet, the SO_2 absorption by $Ca(OH)_2$ had reached saturation. The reaction gas was then switched to 2000 ppm SO_2 + 100 ppm SO_3 (5% O_2, N_2 as balance) for another 60 min. The conversion of $Ca(OH)_2$ by absorbing SO_3 and SO_2 as a function of time during the reactions is shown in Fig. 7. After the addition of SO_3 at 60 min, the conversion of $Ca(OH)_2$ by absorbing SO_3 continued to increase, indicating the occurrence of the SO_3 absorption

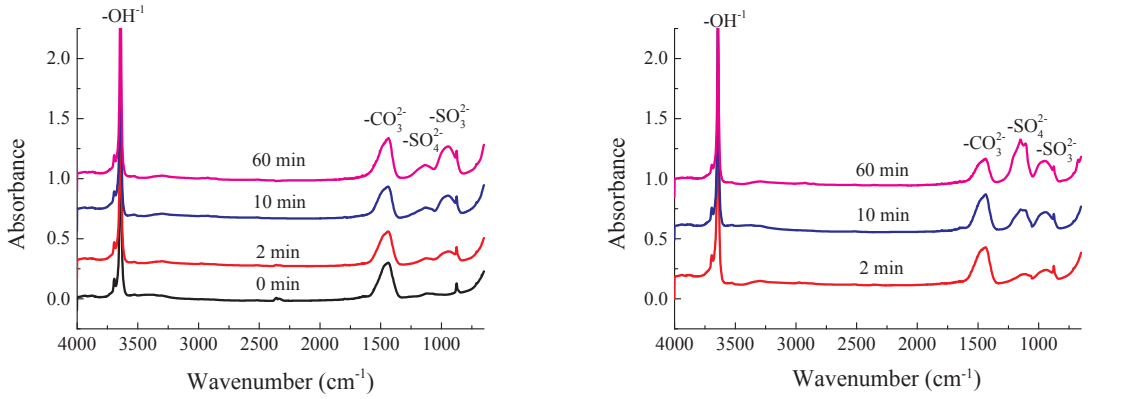

(a) FTIR spectrum of SO_2 absorption by $Ca(OH)_2$ (b) FTIR spectrum of SO_2 and SO_3 absorption by $Ca(OH)_2$

Fig. 5. The functional groups of the desulfurization products at different reaction times. (Pretreatment: absorption by $Ca(OH)_2$ in the SO_X absorption reactor at 300 °C (a) 2000 ppm SO_2; (b) 2000 ppm SO_2 + 100 ppm SO_3 0/2/10/60 min).

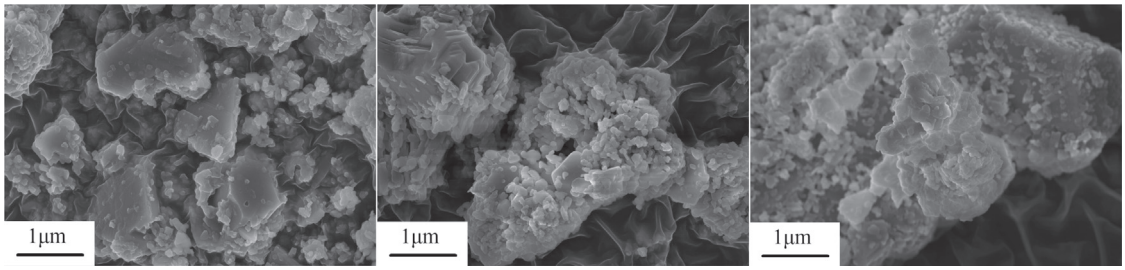

(a) The original $Ca(OH)_2$ (b) 2000 ppm SO_2, 60 min (c) 2000 ppm SO_2+100 ppm SO_3,60 min

Fig. 6. The surface morphology of the original $Ca(OH)_2$ and the desulfurization products.

Table 2
Specific surface area (BET) and specific pore volume (BJH) of the original $Ca(OH)_2$ and the desulfurization products.

	$Ca(OH)_2$	+2000 ppm SO_2 60 min	+2000 ppm SO_2 + 100 ppm SO_3 60 min
BET (m^2/g)	19.9	18.6	14.5
BJH (cm^3/g)	0.077	0.059	0.050

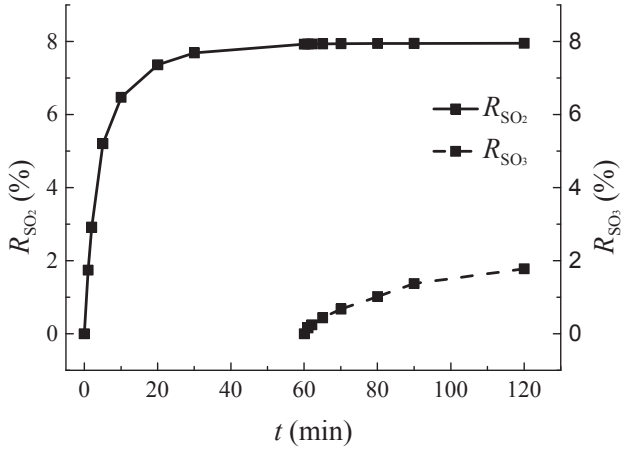

Fig. 7. The possibility of SO_3 reacting with $CaSO_3$. (300 °C, $Ca(OH)_2$, supplying the reaction gas of 2100 ppm SO_2 for 60 min, supplying the reaction gas of 2000 ppm SO_2 + 100 ppm SO_3 for another 60 min).

reaction. However, the conversion of $Ca(OH)_2$ by absorbing SO_2 did not change, indicating that the products which absorbed SO_2 to saturation did not resorb or replace SO_2. Therefore, SO_3 did not react with $CaSO_3$ at 300 °C.

Second, the possibility of SO_3 reacting with $CaSO_4$ to form $Ca(HSO_4)_2$ was verified. A total of 100 mg anhydrous $CaSO_4$ (Aladdin, sample content ≥99.99%) was placed in the SO_X absorption reactor and used to absorb the reaction gas of 2000 ppm SO_2 + 300 ppm SO_3 (5% O_2, N_2 as balance) for 60 min at 300 °C. A total of 10 mg of the products was taken for a temperature-programmed experiment with TGA. The products were heated from 105 °C to 700 °C at a heating rate of 30 °C/min and insulated for 20 min, and then, they were heated from 700 °C to 1300 °C at a heating rate of 30 °C/min and insulated for 20 min under a gas flow of argon at a flow rate of 100 mL/min. The results of TGA experiments showed that the TG curves of the original $CaSO_4$ and the products which contacted SO_3 for 60 min almost completely overlapped, and all of them decomposed at 1200–1300 °C. The decomposition amounts were 11.26% and 11.29%, respectively, with a difference of 0.03%. Therefore, SO_3 did not react with $CaSO_4$ at 300 °C.

Third, the possibility of SO_3 reacting with $CaCO_3$ to form $CaSO_4$ was verified. A total of 100 mg $CaCO_3$ (Sinopharm Chemical Reagent Co., Ltd., sample content ≥ 99.99%) was placed in the SO_X absorption reactor and used to absorb two reaction gases of 2300 ppm SO_2 and 2000 ppm SO_2 + 300 ppm SO_3 (5% O_2, N_2 as balance) for 90 min, respectively, at 300 °C. The original $CaCO_3$, the SO_2 absorption products, and the SO_2 + SO_3 absorption products were taken for temperature-programmed experiments with TGA. The products were heated from 105 °C to 800 °C at a heating rate of 30 °C/min and insulated for 20 min and then heated from 800 °C to 1300 °C at a heating rate of 30 °C/min and insulated for 20 min under a gas flow of argon at a flow rate of 100 mL/min. The results of TGA experiments showed that the TG curves of the original $CaCO_3$ and the SO_2 absorption products almost completely overlapped, and all of them decomposed at 550–800 °C, corresponding to the decomposition of $CaCO_3$. However, the SO_2 + SO_3 absorption products not only had the corresponding $CaCO_3$ decomposition in the temperature range of 550–800 °C but also had an insignificant decomposition at 1200–1300 °C, corresponding to the decomposition of $CaSO_4$. Therefore, SO_3 did react with $CaCO_3$ at 300 °C. However, the conversion of $CaCO_3$ by absorbing SO_3 was only 0.8% at the reaction gas of 2000 ppm SO_2 + 300 ppm SO_3 for 90 min, indicating a poor reactivity between $CaCO_3$ and SO_3. In addition, as an impurity, $CaCO_3$ had a low content in $Ca(OH)_2$. As a result, the contribution of the reaction between SO_3 and $CaCO_3$ was negligible for the continuous SO_3 absorption after the cessation of the SO_2 absorption.

The above three verification experiments showed that the components on the reacted $Ca(OH)_2$ surface could not continue to react with SO_3, and the continuous SO_3 absorption after the cessation of the SO_2 absorption should be due to the transformation of the product layer diffusion mechanism. It is no longer the SO_3 inward diffusion through the product layer, but the ionic diffusion. Fan et al. discovered the ionic diffusion mechanism through the product layer when studying the reaction of CaO and CO_2 or SO_2 + O_2 [35,36]. Taking the reaction of CaO and SO_2 + O_2 at 1300 °C as an example, $CaSO_3$ formed on the CaO surface was rapidly oxidized to $CaSO_4$, and then, a thin layer of $CaSO_4$ was on the CaO surface. First, the Ca^{2+} cations and the O^{2-} anions of the unreacted CaO diffused to the surface of the $CaSO_4$ product layer. Second, the gaseous SO_2 reacted with the O^{2-} anions to form the SO_3^{2-} anion groups, and SO_3^{2-} anion groups were rapidly oxidized to SO_4^{2-} anion groups. Finally, the SO_4^{2-} anion groups reacted with Ca^{2+} cations to form a new $CaSO_4$. However, in this paper, the reaction temperature was 300 °C, and the SO_2 absorption by $Ca(OH)_2$ was almost terminated after 30 min, indicating a lesser effect of the ionic diffusion. The ions were diffused by intrinsic thermal defects in the solid-phase. The higher the temperature, the higher the thermal defect concentration, and the more pronounced the effect of the ionic diffusion. The reaction temperature herein was low, and the ionic intrinsic diffusion was negligible. It is speculated that the adsorbed SO_3 on the surface of the product layer formed a strong potential to drive the ionic migration, causing the Ca^{2+} cations and the OH^- anions of the unreacted $Ca(OH)_2$ migrated to the SO_3 adsorption site through the $CaSO_4$ product layer, thereby promoting the continuous absorption of SO_3.

4. Conclusion

The competitive absorption of SO_3 and SO_2 by $Ca(OH)_2$ was studied with a SO_3 generation/SO_X absorption reaction system. Similar as the common deSO_2 process, the absorption of SO_3 and SO_2 consists of two stages, *i.e.* the chemical kinetics-controlled and product layer diffusion-controlled. In the chemical kinetics-controlled stage, the SO_3 and SO_2 removal efficiencies were around 90% and 55% at the beginning and then decreased; the conversion of $Ca(OH)_2$ by absorbing SO_3 or SO_2 increased fast, with the SO_3 selectivity around 0.1 at the beginning and then increasing with time. In the product layer diffusion-controlled stage, the SO_3 removal efficiency gradually decreased but kept greater than 10%, while the SO_2 removal efficiency deceased to zero; the conversion of $Ca(OH)_2$ by absorbing SO_3 kept increasing with a slower rate, while the conversion of $Ca(OH)_2$ by absorbing SO_2 gradually reached a constant after approximately 30 min, indicating the cessation of the reaction; the SO_3 selectivity continued to increase and reached 0.28, 0.19, 0.13 and 0.31 for the four atmospheres when SO_2 absorption ceased. There existed significant competition between SO_3 and SO_2 absorption. The increasing SO_2 concentration decreased the SO_3 removal efficiency and the selectivity of $Ca(OH)_2$ for SO_3 absorption while the increasing SO_3 concentration increased them.

The absorption products were characterized by FTIR, SEM and Surface Area and Porosity Analyzer. The sulfur-containing functional groups of SO_4^{2-} and SO_3^{2-} were found when the SO_2 and O_2 absorbed on the $Ca(OH)_2$ surface. The absorption of SO_3 increased the intensity of the SO_4^{2-} band, decrease the intensity of the SO_3^{2-} band, and made the product layer more compact.

The mechanism of the continuous SO_3 absorption after the cessation of the SO_2 absorption was explored. The possibility of SO_3 reacting with the components ($CaSO_3$, $CaSO_4$ and $CaCO_3$) on the reacted $Ca(OH)_2$ surface was analyzed. Ionic diffusion was proposed as the main mechanism of the continuous SO_3 absorption after the formation of a dense product layer.

The significant competition between SO_3 and SO_2 absorption decreases the SO_3 removal efficiency and the absorbent utilization. Thus, absorbents with high selectivity for SO_3 absorption need to be developed to reduce the deSO_3 cost.

Notes

The authors declare no competing financial interest.

Acknowledgment

This work was supported by funds from the National Key Research and Development Program of China (2017YFC0210704).

References

[1] Srivastava RK, Miller CA, Erickson C, Jambhekar R. Emissions of sulfur trioxide from coal-fired power plants. J Air Waste Manage Assoc 2004;54(6):750–62.
[2] Forzatti P. Present status and perspectives in de-NOx SCR catalysis. Appl Catal A-Gen 2001;222(1–2):221–36.
[3] Schwämmle T, Bertsche F, Hartung A, Brandenstein J, Heidel B, Scheffknecht G. Influence of geometrical parameters of honeycomb commercial SCR-DeNOx-catalysts on DeNOx-activity, mercury oxidation and SO_2/SO_3-conversion. Chem Eng J 2013;222:274–81.
[4] Duan L, Duan Y, Sarbassov Y, Li Y, Anthony EJ. SO_3 formation under oxy-CFB combustion conditions. Int J Greenh Gas Con 2015;43:172–8.
[5] Xiang B, Zhang M, Wu Y, Yang H, Zhang H, Lu J. Experimental and modeling studies on sulfur trioxide of flue gas in a coal-fired boiler. Energy Fuels 2017;31(6):6284–97.
[6] Cordtz R, Schramm J, Rabe R. Investigating SO_3 formation from the combustion of heavy fuel oil in a four-stroke medium-speed test engine. Energy Fuels 2013;27(10):6279–86.
[7] Xiang B, Shen W, Zhang M, Yang H, Lu J. Effects of different factors on sulfur trioxide formations in a coal-fired circulating fluidized bed boiler. Chem Eng Sci 2017;172:262–77.
[8] Kikuchi R. Environmental management of sulfur trioxide emission: impact of SO_3 on human health. Environ Manage 2001;27(6):837–44.
[9] Brachert L, Kochenburger T, Schaber K. Facing the sulfuric acid aerosol problem in flue gas cleaning: pilot plant experiments and simulation. Aerosol Sci Technol 2013;47(10):1083–91.
[10] Mertens J, Bruns R, Schallert B, Faniel N, Khakharia P, Albrecht W, et al. Effect of a gas-gas-heater on H_2SO_4 aerosol formation: implications for mist formation in amine based carbon capture. Int J Greenh Gas Con 2015;39:470–7.
[11] Cao Y, Zhou H, Jiang W, Chen CW, Pan WP. Studies of the fate of sulfur trioxide in coal-fired utility boilers based on modified selected condensation methods. Environ Sci Technol 2010;44(9):3429–34.
[12] Fleig D, Andersson K, Johnsson F. Influence of operating conditions on SO_3 formation during air and oxy-fuel combustion. Ind Eng Chem Res 2012;51:9483–91.
[13] Spörl R, Walker J, Belo L, Shah K, Stanger R, Maier J, et al. SO_3 emissions and removal by ash in coal-fired oxy-fuel combustion. Energy Fuels 2014;28(8):5296–306.
[14] Bin H, Lin Z, Yang Y, Fei L, Cai L, Linjun Y. PM2.5 and SO_3 collaborative removal in electrostatic precipitator. Powder Technol 2017;318:484–90.
[15] Yang Z, Zheng C, Zhang X, Zhou H, Silva AA, Liu CT, et al. Challenge of SO_3 removal by wet electrostatic precipitator under simulated flue gas with high SO_3 concentration. Fuel 2018;217:597–604.
[16] Huang R, Yu R, Wu H, Pan D, Zhang Y, Yang L. Investigation on the removal of SO_3 in ammonia-based WFGD system. Chem Eng J 2016;289:537–43.
[17] Blythe GM. Furnace injection of alkaline sorbents for sulfuric acid removal. URS Corp report; 2004.
[18] Blythe GM, Dombrowski K. SO_3 mitigation guide update. US EPRI report 1004168; 2004.
[19] Kocaefe D, Karman D, Steward FR. Comparison of the sulfation rates of calcium, magnesium and zinc oxides with SO_2 and SO_3. Can J Chem Eng 1985;63(6):971–7.
[20] Galloway BD, Sasmaz E, Padak B. Binding of SO_3 to fly ash components: CaO, MgO, Na_2O and K_2O. Fuel 2015;145:79–83.
[21] Wang H, Chen D, Li Z, Zhang D, Cai N, Yang J, et al. SO_3 Removal from flue gas with $Ca(OH)_2$ in entrained flow reactors. Energy Fuels 2018;32(4):5364–73.
[22] Wang Z, Huan Q, Qi C, Zhang L, Cui L, Xu X, et al. Study on the removal of coal smoke SO_3 with CaO. Energy Procedia 2012;14:1911–7.
[23] Galloway B, Padak B. Effect of flue gas components on the adsorption of sulfur oxides on CaO (100). Fuel 2017;197:541–50.
[24] Chen P, Wang ZQ, Chang JC, Ma CY. Experimental study of the reactivity of Ca-based matters with SO_3. Proceedings of Power and Energy Engineering Conference. New York: ASME; 2011. p. 1–4.
[25] Moretti AL, Triscori RJ, Ritzenthaler DP. A system approach to SO_3 mitigation. Combined Power Plant Air Pollutant Control Mega Symposium. Washington, DC: Air and Waste Management Association; 2006. p. 1–7.
[26] Results of full-scale testing of sodium bisulfite injection for flue gas sulfuric acid control. US EPRI report, 1004167; 2002.
[27] Rasmussen MH, Wedel S, Pedersen KH, Illerup JB, Dam-Johansen K. Initial reaction between CaO and SO_2 under carbonating and non-carbonating conditions. Chem Eng Sci 2015;134:169–77.
[28] Sun P, Grace JR, Lim CJ, Anthony EJ. Removal of CO_2 by calcium-based sorbents in the presence of SO_2. Energy Fuels 2007;21(1):163–70.
[29] Li Y, Buchi S, Grace JR, Lim CJ. SO_2 removal and CO_2 capture by limestone resulting from calcination/sulfation/carbonation cycles. Energy Fuels 2005;19(5):1927–34.
[30] Manovic V, Anthony EJ. Competition of sulphation and carbonation reactions during looping cycles for CO_2 capture by CaO-based sorbents. J Phys Chem A 2010;114(11):3997–4002.
[31] Xiong J, Li Y, Wang J, Yang Y, Zhu T. Evaluation of sulfur trioxide detection with online isopropanol absorption method. J Environ Sci-China 2018;72:25–32.
[32] García-Martínez J, Bueno-López A, García-García A, Linares-Solano A. SO_2 retention at low temperatures by $Ca(OH)_2$-derived CaO: a model for CaO regeneration. Fuel 2002;81(3):305–13.
[33] Luo C, Zheng Y, Guo J, Feng B. Effect of sulfation on CO_2 capture of CaO-based sorbents during calcium looping cycle. Fuel 2014;127:124–30.
[34] Ishizuka T, Kabashima H, Yamaguchi T, Tababe K, Hattori H. Initial step of flue gas desulfurization – an IR study of the reaction of SO_2 with NO_X on CaO. Environ Sci Technol 2000;34(13):2799–803.
[35] Sun Z, Luo S, Qi P, Fan LS. Ionic diffusion through Calcite ($CaCO_3$) layer during the reaction of CaO and CO_2. Chem Eng Sci 2012;81:164–8.
[36] Hsia C, St Pierre GR, Raghunathan K, Fan LS. Diffusion through $CaSO_4$ formed during the reaction of CaO with SO_2 and O_2. AIChE J 1993;39(4):698–700.